JOURNAL OF AIRCRAFT
Vol. 42, No. 5, September–October 2005

Tip Vortex Behind a Wing Oscillated with Small Amplitude

D. Birch* and T. Lee†
McGill University, Montreal, Quebec H3A 2K6, Canada

The effect of reduced frequency on the tip vortex in the near field behind a NACA 0015 wing oscillated sinusoidally within the static-stall angle (= 14 deg) was investigated at $Re = 1.86 \times 10^5$. The nearly symmetric vortex was observed at 0.5 to 1.5 chords downstream of the trailing edge similar to the case of a stationary wing. The oscillating wing produced a less concentrated vortex of similar diameter and had a larger radial gradient in circulation strength, compared to that of a stationary wing, for reduced frequency less than about 0.1. The axial-flow velocity was always wake-like, with its minimum value increasing with the reduced frequency. The peak value of the vorticity and the vortex strength and the lift-induced drag were higher during pitch-down than during pitch-up. The normalized circulation in the inner part of the axisymmetric vortex also exhibited a self-similar structure, which was insensitive to the reduced frequency. The induced drag increased with the reduced frequency.

Nomenclature

b	=	wing span
C_d	=	drag coefficient
C_{Di}	=	induced drag coefficient, $= D_i/\frac{1}{2}\rho u_\infty^2 bc$
$C_{D,3\text{-}d}$	=	total drag coefficient of a three-dimensional wing configuration
$C_{L,2\text{-}d}$	=	lift coefficient of a two-dimensional wing configuration, $=$ Lift$/\frac{1}{2}\rho u_\infty^2 bc$
C_l	=	lift coefficient
c	=	airfoil chord
$D_{3\text{-}d}$	=	total drag of a three-dimensional wing configuration
D_i	=	induced drag
Re	=	chord Reynolds number, $= u_\infty c/\nu$
r	=	radial position
r_c	=	core radius at which $v_\theta = v_{\theta\,\max}$
r_o	=	vortex outer radius
s	=	multiple-hot-film sensor spacing
t	=	time
u	=	axial velocity
u_∞	=	freestream velocity
u'	=	fluctuating axial velocity
v	=	transverse mean velocity
v_θ	=	tangential or swirl velocity
w	=	spanwise mean velocity
x	=	streamwise or axial direction
y	=	transverse direction
z	=	spanwise direction
α	=	angle of attack
Γ	=	circulation or vortex strength
Γ_c	=	core circulation
Γ_0	=	total circulation
ζ	=	streamwise vorticity
ν	=	kinematic viscosity
ρ	=	density
σ	=	source term in Eq. (3)
τ	=	phase, $= \omega t = 2\pi f t$
ϕ	=	velocity potential
ψ	=	stream function

Received 31 May 2004; revision received 27 July 2004; accepted for publication 28 July 2004.

*Ph.D. Research Assistant, Department of Mechanical Engineering.
†Associate Professor, Department of Mechanical Engineering. Member AIAA.

I. Introduction

THE counter-rotating longitudinal vortices generated by aircraft wing tips, because of their hazardous effects on flight safety and airport efficiency, continue to be of concern to the aviation industry and aircraft manufacturers alike. Moreover, tip vortices shed from helicopter rotor blades and propellers interact with following blades, causing rotor noise and vibration. Extensive investigations have been conducted to characterize the flow structure of the tip vortex and its dissipation or persistence, as well as its control in the mediate or far-field regions behind a stationary wing. However, only limited investigations[1–8] have been reported to document the evolution and turbulence structure of the tip vortex and the development of the axial and tangential velocities with the downstream distance in the near field (up to three chord lengths downstream of the trailing edge of the wing), which is significant in both fixed- and rotary-wing aerodynamics. Meanwhile, much less attention has been given to the tip vortex generated by an oscillating wing,[9–11] which is of practical significance to the rotorcraft aerodynamics.

The flow around a sinusoidally oscillating airfoil, especially the transient phenomena of dynamic stall and the airload-loop hysteresis on airfoils and lifting surfaces, has been studied extensively both numerically and experimentally.[12–17] The retreating-blade dynamic stall problems of helicopters, a well-known limiting factor for the high-speed performance of modern helicopters that is accompanied by large lift unsteadiness and torsional loadings, have been recognized and received considerable attention. The predominant feature of dynamic stall is the formation and shedding and convection over the upper surface of the airfoil of a vortex-like disturbance, that is, the leading-edge vortex (LEV), from the leading edge of the airfoil, which induces a nonlinearly fluctuating pressure field and produces transient variations in forces and moments that are fundamentally different from their steady-state counterparts. After the energetic LEV passes off the trailing edge, the flow progresses to a state of full separation over the upper surface and is accompanied by a sudden loss of lift and decrease in pitching moment. Also, depending on the values of the reduced frequency and the amplitude, the massive LEV separation, as a result of the catastrophic detachment of the LEV from the upper-wing surface as a result of the adverse-pressure-gradient effects imposed on the boundary-layer flow, happens either near the end of pitch-up motion or at the beginning of the pitch-down motion. An excellent review is given by McCroskey.[16]

Recently, the spatial-temporal progression of the boundary-layer transition, flow reversal, separation and reattachment, and the behavior of the LEV were pinpointed and characterized both nonintrusively and simultaneously by Lee et al.[12,14] by using multiple hot-film sensor (MHFS) arrays. Lee et al. also observed that the hysteresis in the dynamic-load loops was attributed to the asymmetry that existed between the occurrence of separation and reattachment. It is believed that these unsteady boundary layer and stall

events have a significant influence on the flow structure of the tip vortex and that the hysteresis and phase shift are two important causes for a tip vortex behind an oscillating wing to deviate from the commonly observed behavior of a tip vortex behind a stationary wing at the same incidence. So far, only three refereed experimental investigations,[9–11] the author's knowledge, with a limited frequency and amplitude range, have been reported. The effects of the oscillation frequency and amplitude on the behavior of the tip vortex during a cycle of oscillation demand further investigation.

The near-field wing-tip vortex behind a stationary wing, for $0 < x/c < 1$, was first examined by Freymuth et al.[9] through flow-visualization studies, where x is the streamwise distance downstream of the trailing edge and c is the chord of the wing. The flow in this region was found to be highly three dimensional and exhibited strong spatial velocity gradients. Ramaprian and Zheng[10] studied the near field of the tip vortex behind an oscillating NACA 0015 rectangular wing with a square tip by using a three-component laser Doppler anemometer at a chord Reynolds number Re of 1.8×10^5 with $\alpha(t) = 10\,\text{deg} + 5\,\text{deg}\sin(2\pi f t)$ (i.e., the light-stall oscillation case[14,16]) and a reduced frequency $\kappa (= \pi f c/u_\infty$, where f is the oscillation frequency and u_∞ is the freestream velocity) of 0.1. They explored the unsteady velocity and vorticity fields associated with the evolving tip vortex in the near field for $0.16 < x/c < 2.66$ and observed that the average trajectory of the oscillating tip vortex was very nearly the same as for a stationary wing at the mean incidence. They also reported that the length and circulation scales, as well as the maximum circulation carried by the vortex flow under the conditions studied, were modulated in a significantly nonquasisteady manner. The normalized circulation distribution across most of the inner part of the vortex for $x/c > 0.7$, however, exhibited the same universal behavior as the vortex behind a stationary wing. More recently, Chang and Park[11] examined the hysteretic behavior of the wake behind a NACA 0012 airfoil oscillated with $\alpha(t) = 15\ \text{deg} + 15\ \text{deg}\sin(2\pi f t)$ (i.e., the deep-stall oscillation case[14,16]) at $\kappa = 0.09$ for $Re = 3.4 \times 10^4$ by using a triple hot-film probe at $x/c = 0.5$ and 1.5. Chang and Park found that the size of the vortex core was larger, and the peak tangential velocity and the axial velocity deficit were smaller during pitch-down than during pitch-up. Also, because of the massive LEV flow separation, the circulation or vortex strength of the tip vortex at a given α was greater during pitch-up than during pitch-down. Moreover, the vortex regions in all of the cases suffered from an axial velocity deficit.

In summary, it is now well-known that the magnitudes of the oscillation frequency and amplitude lead to the complex unsteady flow phenomena and the large variations in the airloads; however, much work is still needed to better understand and control the tip vortex generated behind an oscillating wing under the influence of different frequencies and amplitudes. The objective of this study was to characterize the phase-locked ensemble-averaged velocity and vorticity distributions and turbulence structure and the strength and size of the tip vortex generated by a NACA 0015 airfoil oscillated with $\alpha(t) = 0 + 6\,\text{deg}\sin(2\pi f t)$ (i.e., the attached-flow oscillation case[12,14]) for $x/c = 0.5$, 1, and 1.5 and $\kappa = 0.09$ to 0.18 at $Re = 1.86 \times 10^5$ by using a triple hot-wire probe and a seven-hole pressure probe. Lift-induced drag D_i was also computed and was compared to the wind-tunnel force-balance data.

II. Experimental Apparatus and Methods

The experiment was carried out in the $0.9 \times 1.2 \times 2.7$ m suction-type subsonic wind tunnel in the Department of Mechanical Engineering at McGill University with a freestream turbulence intensity of 0.08% at 35 m/s. A square-tipped, rectangular NACA 0015 wing with a chord of 20.3 cm and a span b of 50.1 cm was used to generate the tip vortex (Fig. 1). The aspect ratio of the half-model wing was 2.5. The wing model was mounted horizontally at the center of the sidewall of the wind-tunnel test section. A $0.48 \times 60 \times 60$ cm aluminum endplate with sharp leading edges was fixed to the sidewall of the test section. The gap between the wing and the endplate was kept at less than 1 mm to minimize the leakage of flow through the gap. The origin of the coordinate system was located at the trailing edge of the wing with the x, y, and z axes in the streamwise, transverse, and spanwise directions, respectively. A servomotor was used to provide the sinusoidal motion of the wing about its quarter-chord. The mean incidence and the amplitude of the oscillation were set at 0 and 6 deg, respectively. The reduced frequency was set at $\kappa = 0.09$, 0.12, and 0.18. Information on the phase angle and instantaneous direction of the wing motion (i.e., pitch-up or pitch-down) during the oscillation cycle was obtained from both the servomotor feedback encoder and a potentiometer mounted on the servomotor shaft. Also, in the following discussion the suffix u is used to indicate pitch-up when α is increasing, and d is used to indicate pitch-down when α is decreasing. The instantaneous velocities were subsequently ensemble averaged over 40–80 oscillating cycles to obtain phased-locked averages of the flow properties at various

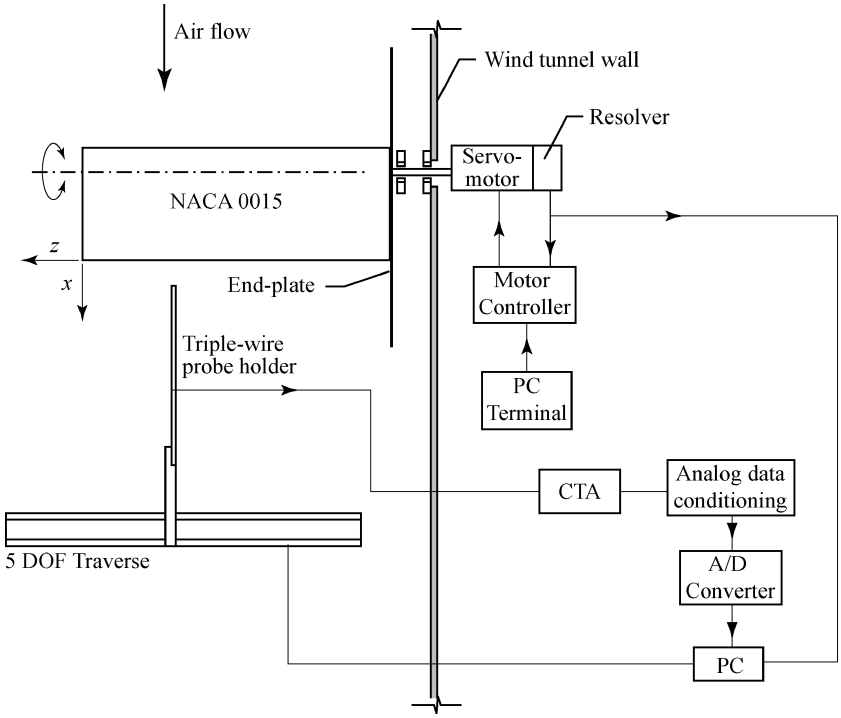

Fig. 1 Schematic of experimental setup.

phase positions during the cycle. A miniature seven-hole pressure probe (with an outside diameter of 2.4 mm) and a miniature triple hot-wire probe (Auspex Model AVEP-3-102) were used to measure the mean and fluctuating velocity components. The pressure probe and triple hot-wire probe were calibrated in situ, following the calibration procedures described by Wenger and Devenport[18] and Chow et al.,[4] respectively, before the installation of the model. The pressure and hot-wire signals were sampled at 500 Hz and were recorded on a PC through a 16-bit A/D converter board. Probe traversing was achieved through a custom-built computer-controlled traversing system with a position resolution in all three directions of 10 μm. Tip-vortex flowfield measurements were made at crossflow planes located $x/c = 0.5$, 1.0, and 1.5. Data planes taken in the near field of the wing models had 33×33 measuring grid points with an increment of $\Delta y = \Delta z = 3.2$ mm. The freestream velocity was fixed at 14.4 m/s, which rendered a chord Reynolds number of 1.86×10^5.

For lift and drag force measurements, the model was mounted vertically between two $0.45 \times 60 \times 60$ cm aluminum endplates with sharp leading edges and on an external two-component force balance located below the wind tunnel. Details of the force-balance system are given in Birch and Lee.[7,8] This two-dimensional configuration approximated an airfoil with an effective aspect ratio of infinity and will hereafter be referred to as the two-dimensional wing configuration with $C_{L,2\text{-}d}$ and $C_{D,2\text{-}d}$ denoting the corresponding total lift and drag coefficients, respectively. Furthermore, by removing the top endplate, the total lift coefficient $C_{L,3\text{-}d}$ and drag coefficient $C_{D,3\text{-}d} = C_{\mathrm{Dp}} + C_{\mathrm{Di}}$ (where C_{Dp} is the profile drag coefficient and C_{Di} is the lift-induced drag coefficient) of a three-dimensional wing configuration were also obtained. The maximum experimental uncertainties in the results reported have been estimated as follows[7,8]: mean velocity 3.5%, vorticity component 8%, vortex radius 4%, and velocity fluctuation 3%. No wind-tunnel wall corrections were made to the present measurements. The vortex meandering was examined by using the correlation technique/criteria employed by Chow et al.[4] It was determined from the correlation measurements that meandering of the vortex was small and did not contribute appreciably to the present measurements.

III. Results and Discussion

A. Phase-Locked Ensemble-Averaged Velocity and Vorticity Distributions

Figure 2 shows the typical nondimensional phase-locked ensemble-averaged crossflow vector plots and the streamwise vorticiy $\zeta c/u_\infty$ and the fluctuating axial-velocity u'/u_∞ contours of

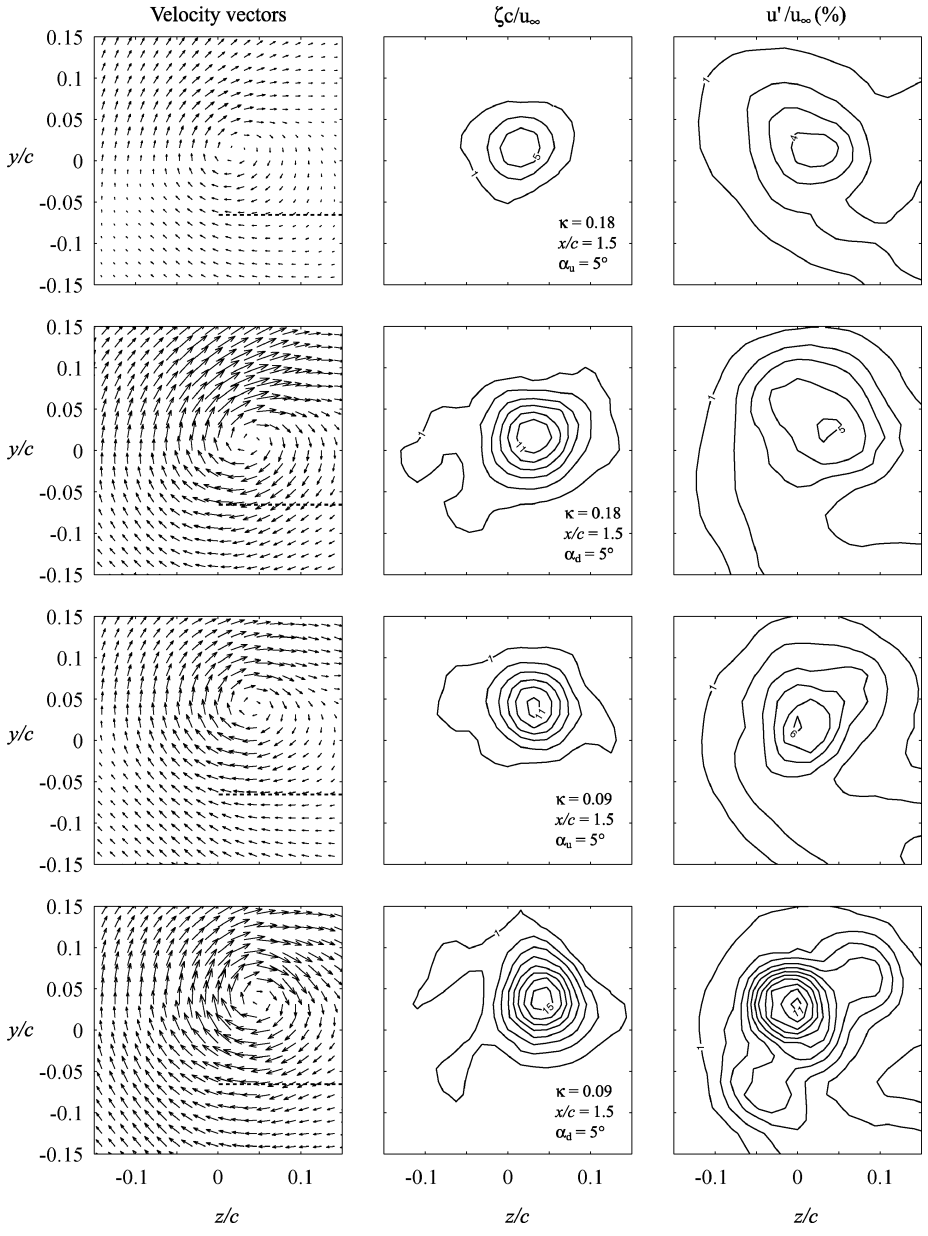

Fig. 2 Nondimensional phase-locked ensemble-averaged *vw*-velocity vector plots and vorticity and axial-velocity fluctuation contours. Numerical values denote ζ_c/u_∞ and u'/u_∞ levels with constant increments of two and one, respectively.

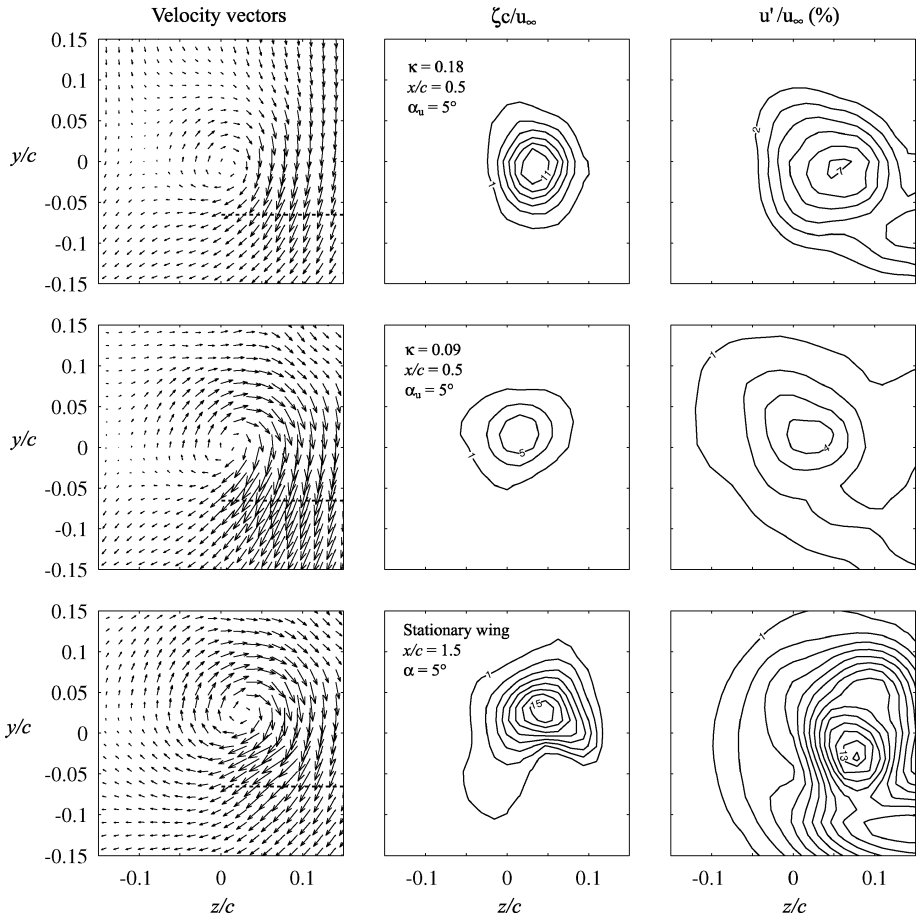

Fig. 2 Nondimensional phase-locked ensemble-averaged *vw*-velocity vector plots and vorticity and axial-velocity fluctuation contours. Numerical values denote ζ_c/u_∞ and u'/u_∞ levels with constant increments of two and one, respectively (continued).

the tip vortex generated by a NACA 0015 wing oscillated with $\alpha(t) = 0\,\text{deg} + 6\,\text{deg}\sin\omega t$ for $\alpha_u = 5$ deg (during pitch-up) and $\alpha_d = 5$ deg (during pitch-down) at $x/c = 0.5$ and 1.5 with $\kappa = 0.09$ and 0.18. Also shown in Fig. 2 are the results of a stationary wing at the same airfoil incidence. The dashed lines denote the instantaneous location of the wing trailing edge. Regardless of the magnitude of the reduced frequency, the majority of the tip vortex flow attained axisymmetry with uniform spacing of the vorticity contours, except for the outermost part of the spiral, during the entire oscillation cycle for $x/c \geq 0.5$, similar to the case of a stationary wing but with varied vortex strength and velocity distributions. Outside the core the flow structure was dominated by the remainder of the wing wake as can be seen clearly from the u' distributions. The vortex center moved with the instantaneous α; it moved slightly inboard from the wing tip and upward (downward) relative to the trailing edge as α increased (decreased) over the oscillation cycle. No LEV and/or massive flow separation were observed for the present low-amplitude attached-flow oscillation case. The tip vortex was of lower (higher) vorticity during pitch-up (pitch-down) for an oscillating wing, compared to that of a stationary wing, though values decreased slightly with the downstream distance but increased with the reduced frequency. A similar trend was also exhibited in the spatial and temporal variations of the mean and fluctuating velocities. The inner region of the vortex was, however, found to be less turbulent but of similar diameter, compared to its static counterparts, and had a larger radial gradient in circulation strength. The spiral (corresponding to the shear layer from the inboard regions of the flow, which was in a process of rolling up to form the axial tip vortex) was generally slightly more organized for the most part during pitch-up motion than during the pitch-down motion.

The variation of the phase-locked ensemble-averaged vortex flow quantities (v_θ, ζ, u, and u') across the vortex with the reduced frequency at $x/c = 1.5$ and $\alpha_u = \alpha_d = 5$ deg is presented in Fig. 3. The tangential velocity profile inside the vortex core was linear and exhibited a maximum at the core radius r_c (defined by the location of the maximum induced tangential velocity) at all angles of attack (Fig. 3a), which are qualitatively similar to those observed in a classical steady viscous trailing vortex in the far field behind a stationary wing.[19] Also, the axisymmetric behavior of the tangential velocity v_θ and ζ (Fig. 3b) in the inner region of the vortex and their decay to nearly zero in the outer part of the vortex, a characteristic of a well-organized and nearly symmetric vortex, were apparent. Figure 3b also shows that the vorticity distribution across the inner region of the vortex, which was a result of viscous and/or turbulent diffusion, varied considerably during the oscillation cycle. The strongest vorticity was observed near the center of the vortex. For the present low-amplitude oscillation, the magnitude of this vorticity (and also the peak tangential velocity) was found to be generally higher during pitch-down and decreased with increasing κ and x/c.

Figure 3c shows that a wake-like axial velocity distribution was observed at $x/c = 1.5$ for $\alpha = 5$ deg for both stationary and oscillating wings; the minimal axial core velocity, however, varied from $0.92u_\infty$ to $0.76u_\infty$, compared to $0.82u_\infty$ for a stationary wing, and increased progressively with α and κ over the oscillation cycle. According to Batchelor,[19] the magnitude of the axial velocity in a trailing vortex is determined by a balance between the energy loss caused by dissipation in the wing boundary layer and the radial gradient in the circulation strength. The results also indicate that the velocity deficit region became narrower, and the magnitude of velocity deficit became smaller during pitch-down, suggesting that the flow during pitch-up separated from the wing upper surface later (than during pitch-up) and led to better mixing and hence less velocity deficit. The axial-velocity fluctuations were found to be significantly lower than the static-wing values, suggesting that for an oscillating wing (Fig. 3d), the tip vortex was less tightly wound and less diffused. The size of vortex core, however, remained basically unchanged, regardless of the reduced frequency, compared to its static counterparts. Figures 4a–4d summarize the typical variation

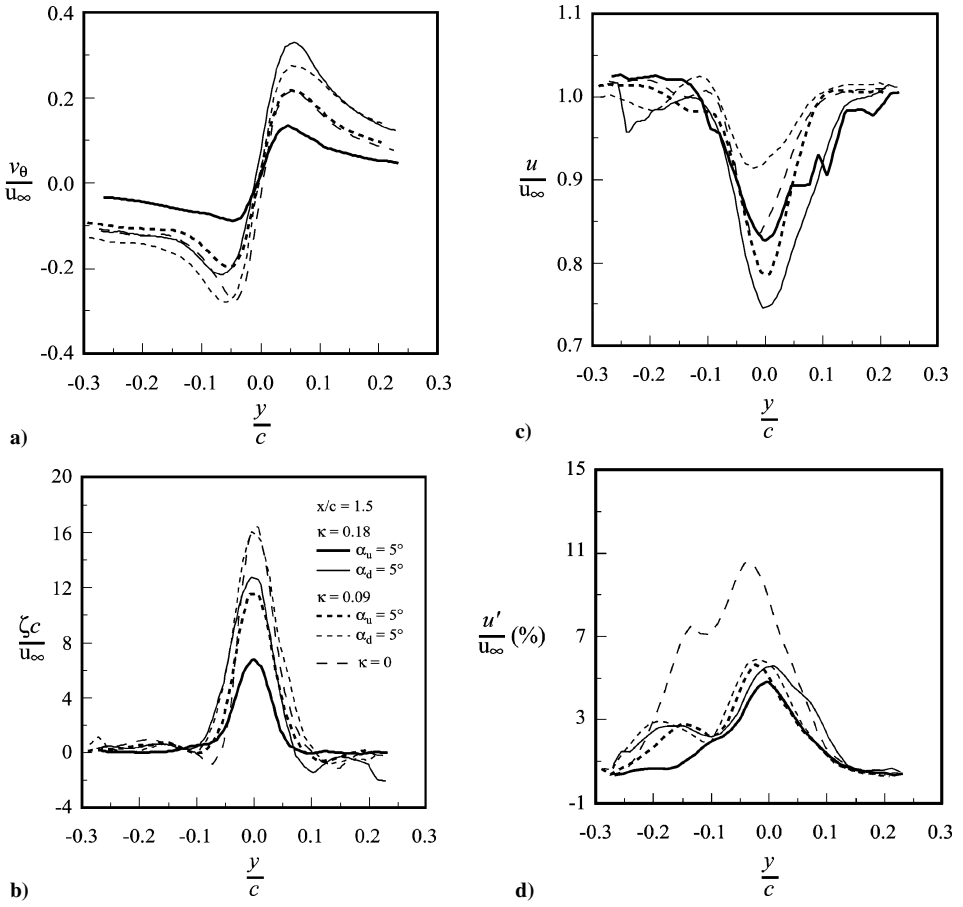

Fig. 3 Typical distributions of the phase-locked ensemble-averaged vortex flow quantities across the vortex.

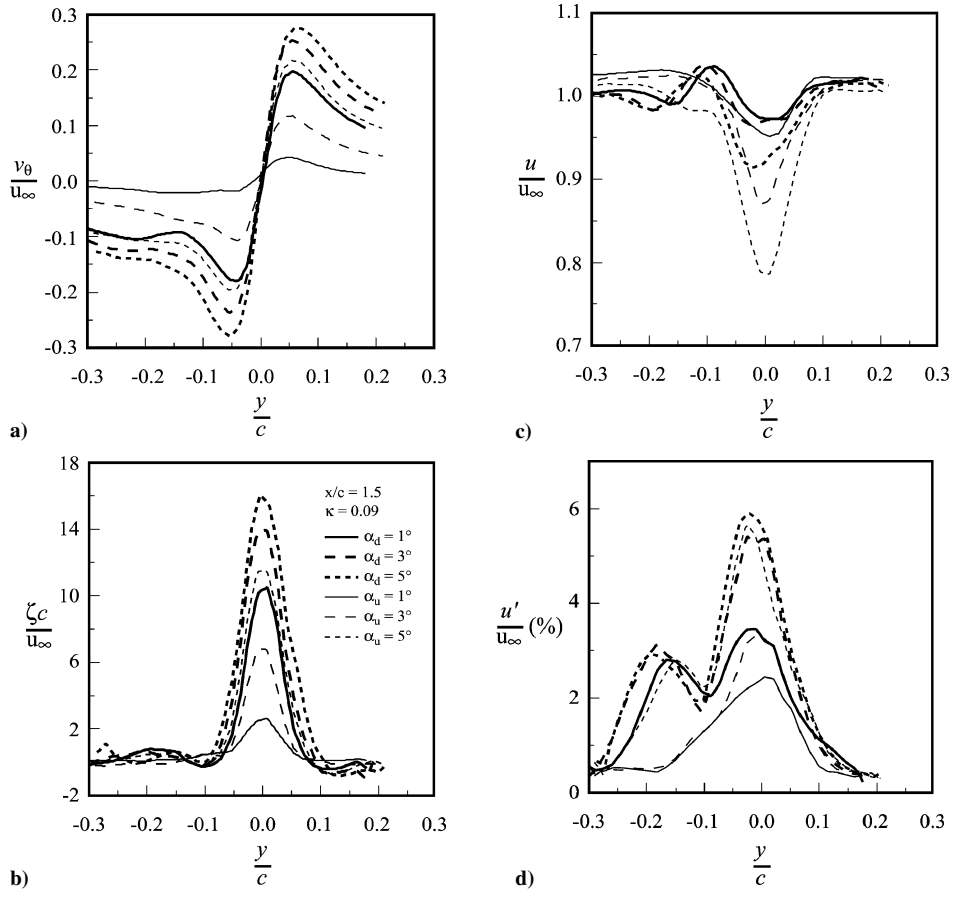

Fig. 4 Composite plots of phase-locked ensemble-averaged vortex flow quantities.

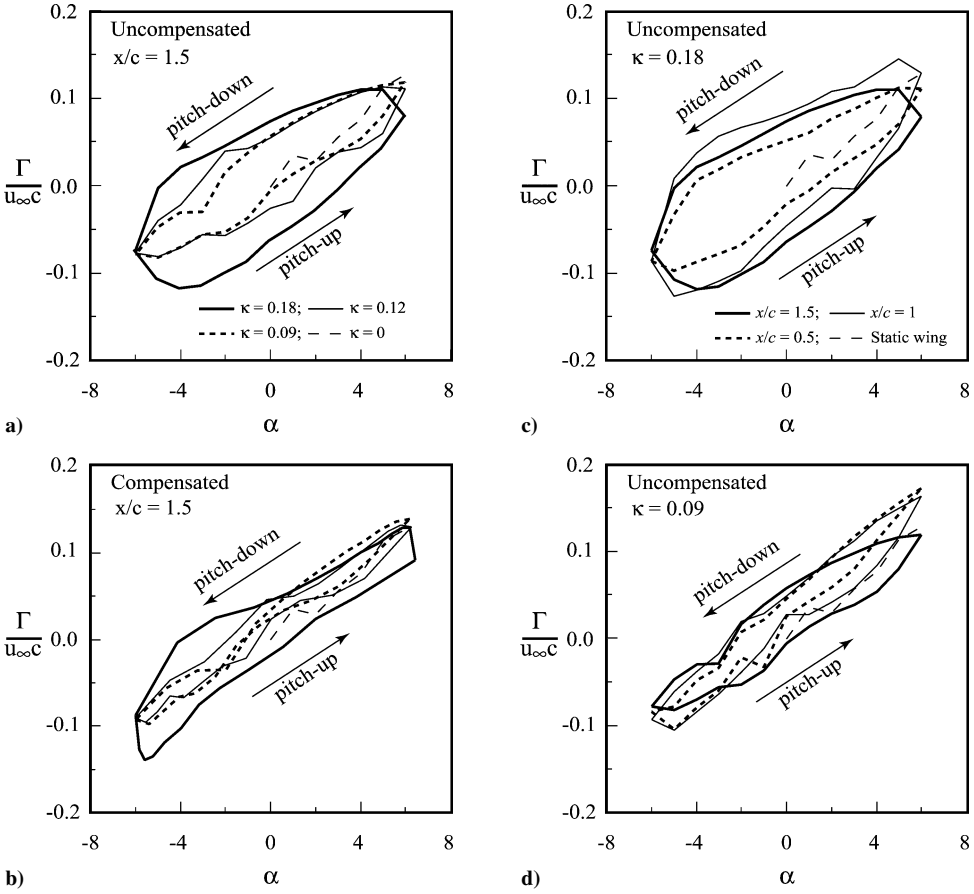

Fig. 5 Variation of phase-locked ensemble-averaged vortex strength over an oscillation cycle.

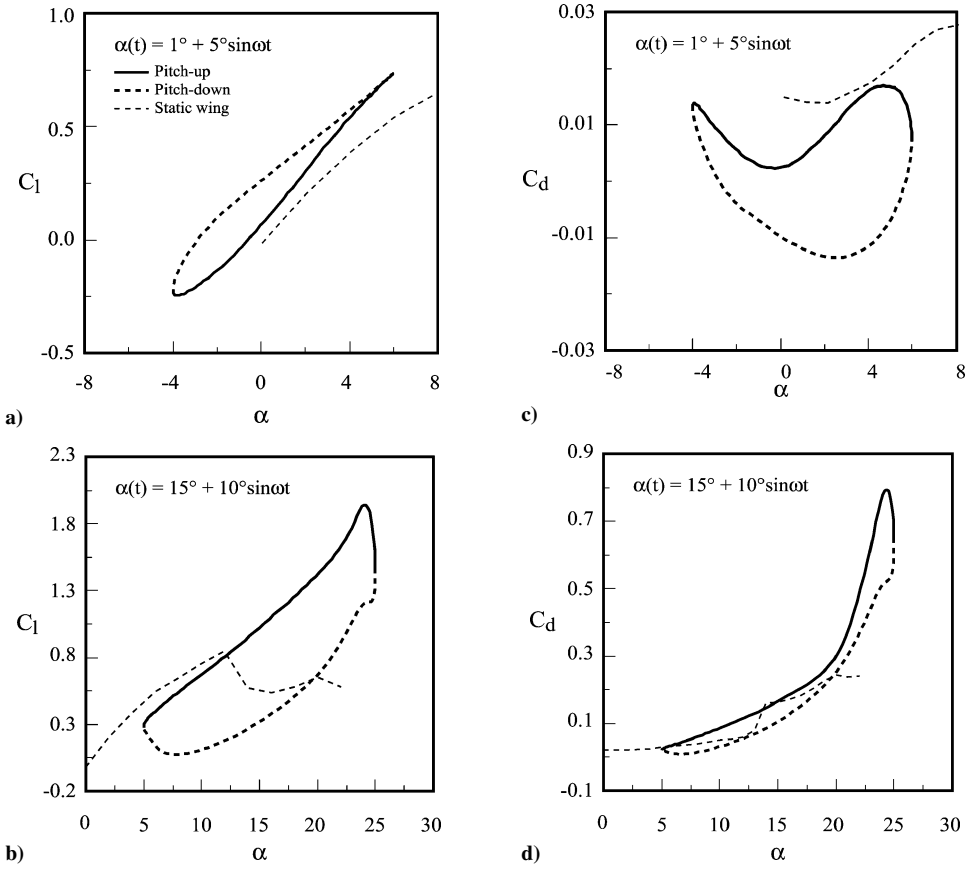

Fig. 6 Dynamic lift and drag loops.

of the phase-averaged vortex flow quantities, across the vortex center for $\alpha_u = \alpha_d = 1$, 3, and 5 deg at $\kappa = 0.09$ and $x/c = 1.5$ during one cycle of oscillation. It is again evident that the peak values of the tangential velocity and vorticity, and the axial-velocity deficit and the fluctuation were found to be higher during pitch-down than during pitch-up, and increased with the instantaneous angle of attack $\alpha(t)$.

B. Behavior of Vortex Strength and Inner Vortex Flow

The spatial-temporal evolution of the phase-locked ensemble-averaged total circulation $\Gamma_0/u_\infty c$ of the tip vortex at different κ, $\alpha(t)$, and x/c over one cycle of oscillation is given in Fig. 5. Also shown in Fig. 5 are the stationary-wing values (denoted by dotted lines). The vortex strength was determined by employing Stokes' theorem to compute the circulation. The computed circulation loops clearly demonstrate the hysteretic property existing between the pitch-up and pitch-down motion, which is similar to the hysteresis observed in the dynamic-load ($C_l - C_d - C_m$ vs α) loops for an oscillating wing.[14,15] Figure 5a shows that at a fixed x/c the level of hysteresis increased with the reduced frequency. The degree of asymmetry or hysteresis was, however, found to be a weaker function of the downstream distance for $\kappa \leq 0.12$ (Figs. 5c and 5d). The circulation in the near field for $\kappa = 0.09$–0.18 was seen to vary approximately linearly with α over a wide range except in the vicinity of the maximum and minimum angles of attack. Both the uncompensated and compensated values of the circulation during pitch-up were smaller than during pitch-down at a given α for small-amplitude oscillations, similar to the hystereses observed in the dynamic C_l and C_d loops reported by Lee and Gerontakos[14] [for a NACA 0012 airfoil oscillated with $\alpha(t) = 1$ deg $+ 5$ deg $\sin\omega t$ and $\kappa = 0.1$; Fig. 6a]. The rates of increase or decrease of the vortex strength per unit angle of attack were, however, about the same for both pitch-up and pitch-down, a phenomenon also observed for dynamic-stall oscillations where the flow was massively separated.[11] The hysteresis became slightly less significant when compensated for phase lag; for clarity, only the uncompensated Γ was presented in Figs. 5c and 5d. The phase-lag compensation scheme followed the suggestion of Chang and Park.[11] A smaller degree of hysteresis was observed for the compensated circulation loops for $\kappa < 0.12$ and with the values of Γ in a close agreement with the static values. This, in a way, ascertains that for small-amplitude oscillations the flow during both pitch-up and pitch-down was generally similar to that of the stationary wing in the present experiment.

The observed lower Γ values during pitch-up than during pitch-down could be attributed to the delay (promotion) of the transition (relaminarization) of the boundary layer, and its subsequent separation from the airfoil upper surface for a rectangular wing oscillated with $\alpha_{\max} \ll \alpha_{ss}$ (Refs. 12 and 14). Figure 7 shows the signals from selected MHFS array outputs from a bank of constant-temperature anemometers. The MHFS array was bonded to the entire NACA 0012 airfoil surface [with a chord of 15 cm and was oscillated with $\alpha(t) = 1$ deg $+ 5$ deg $\sin\omega t$ and $\kappa = 0.1$]. A total of 140 hot-film sensors, which were electron-beam evaporated onto a 50-μm-thick polyimide substrate, with a sensor spacing s of 1.3 mm arranged in a straight-line array, were used to identify the state and behavior of the boundary layer. Sensors S_{122} and S_1 were located at the trailing and leading edges of the airfoil, respectively. The transition and relaminarization were identified directly from the sharp increase (e.g., points ①–② in sensor S_{82} outputs at $s/c = 34.6\%$) and drop (points ③–④) of the MHFS output voltage levels. Points ②–③ indicate the extent of the attached turbulent boundary layer. The lowest curve in Fig. 7 represents the variation in the potentiometer. The sensor numbers shown on the right-side axis denote the location of the sensor along the airfoil upper (S_1–S_{122}) and lower surfaces (S_{123}–S_{140}). Details of the MHFS layout and operation are given by Lee et al.[12,14] Figure 7 shows that during pitch-up the boundary-layer laminar-to-turbulent transition was delayed (compared with a stationary wing) and tended to remain laminar over the majority of the wing surface, which thus rendered a relatively small portion of the boundary-layer flow, in the trailing-edge region, turbulent, and

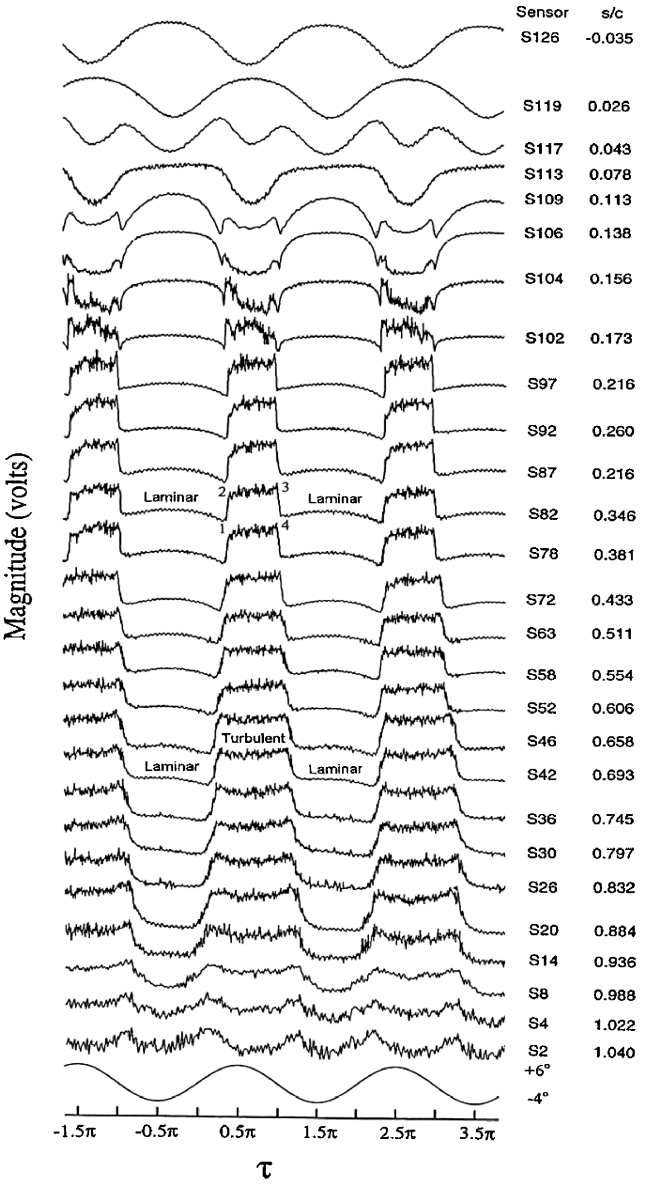

Fig. 7 Selected MHFS outputs.

subsequently resulted in a slightly earlier flow detachment (thus a higher C_d and a lower C_l as presented in Fig. 6a) compared to during pitch-down. During pitch-down, the attached turbulent boundary layer extended over a majority of the wing surface, which better withstood the imposed retardation and separation, detached later from the wing surface and resulted in a smaller and less diffusive wake of a higher Γ. The degree of delay (promotion) of the transition (relaminarization) increased with increasing κ. Figure 6b demonstrates that for large-amplitude oscillations a significantly lowered C_l and an increased C_d (as a result of the massive LEV-induced separation) during pitch-down motion appeared, similar to the observations made by researchers elsewhere.

Figure 8a shows the variation of the nondimensional phase-locked ensemble-averaged circulation $\Gamma(r)/u_\infty c$ with radius r in the vortex for $\alpha(t) = 5$ deg at $x/c = 1.5$ with $\kappa = 0.09$ and 0.18. The observed gradual and monotonic increase in circulation with radial distance in the inner region of the vortex generated by an oscillating wing is very similar to the behavior of a stationary vortex[5,7,8] and is clearly indicative of the viscous/turbulent nature of the vortex. It is seen, however, that the circulation distribution varied considerably during the oscillation cycle and that the individual distributions for a given incidence during pitch-up and pitch-down motions did not correspond with each other. The peak values of Γ_0 also show a small but consistent variation with the distance downstream, as a result

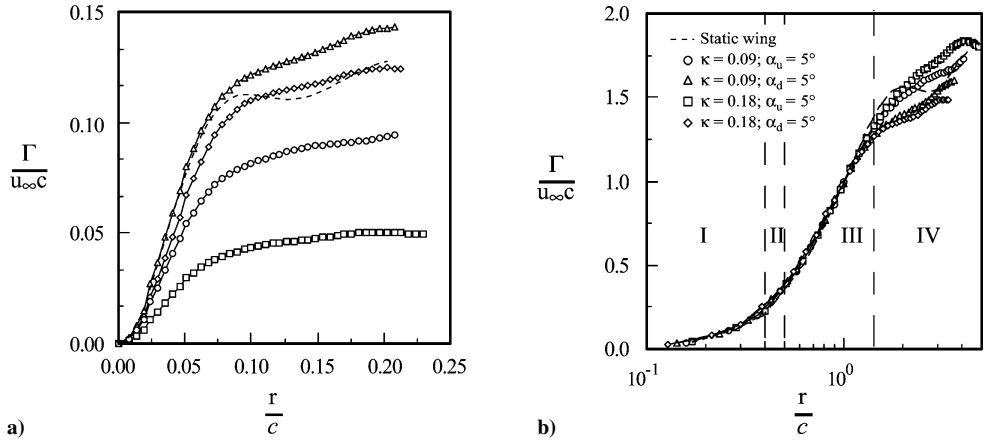

Fig. 8 Phase-locked ensemble-averaged circulation distribution: I, inner-core region; II, buffer region; III, logarithmic region; and IV, outer region.

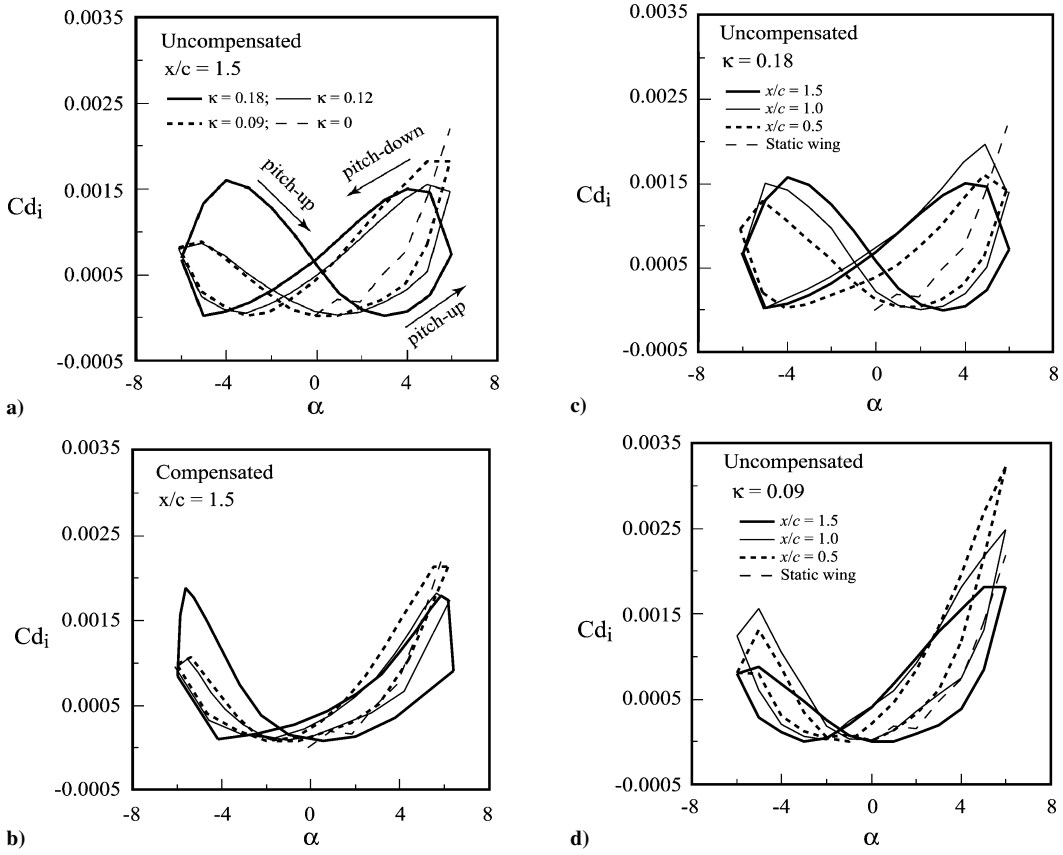

Fig. 9 Variation of induced drag coefficient over an oscillation cycle.

of the continued rollup of the shear layer, which brought with it a small amount of additional axial vorticity into the vortex.

Figure 8b shows the distributions of the phase-locked ensemble-averaged Γ/Γ_c across the vortex plotted in semilogarithmic coordinates $\log(r/r_c)$. Γ_c denotes the circulation of the vortex core. Data are shown only for instantaneous $\alpha(t) = 5$ deg at $x/c = 1.5$ with $\kappa = 0.09$ and 0.18, for the sake of clarity. A large inner region of the highly three-dimensional vortex rolled up quickly in the near field (as shown in Fig. 2), and the layers of the spiral merged rigorously together to result in a nearly symmetric structure. For an oscillating wing, the axisymmetric distributions exhibited self-similarity in the inner region represented by $0 < r/r_c < 1.4$, which coincided with the corresponding distribution observed in the tip vortex behind a stationary wing.[5,7,8] The observed self-similarity in the tip vortex in the near field is of particular interest because it generally takes at least a distance of several tens of wing chords downstream for the vortex to become fully developed and attain the characteristics of asymptotic turbulent trailing vortices. The distribution of the phase-averaged circulation within the tip vortex core followed an $\Gamma \propto r^2$ profile for $r/r_c < 0.4$ and varied logarithmically for $0.5 < r/r_c < 1.4$. For $r/r_c > 1.4$ (denoted by Region IV), the value of Γ continued to vary with x/c, attributed to the fact that the roll-up of the vortex was only nearly complete, and, therefore, there was a slow addition of vorticity to the outer layers of the vortex from the shear layer arriving from the inboard regions. The empirical curve-fit relationships that describe the inner-core region and the logarithmic region, insensitive to κ, $\alpha(t)$, and x/c, are[20,21]

$$\Gamma(r)/\Gamma_c = 1.551(r/r_c)^2 \qquad \text{for} \qquad r/r_c < 0.4 \tag{1}$$

$$\Gamma(r)/\Gamma_c = 2.146\log(r/r_c) + 0.988 \qquad \text{for} \qquad 0.5 < r/r_c < 1.4 \tag{2}$$

Moreover, all of the data within $0 < r/r_c < 1.2$ collapsed together onto a sixth-order polynomial (similar to that of a stationary wing[5,7,8]): $\Gamma(r)/\Gamma_c = 1.717(r/r_c)^2 - 0.938(r/r_c)^4 + 0.215(r/r_c)^6$ with an autocorrelation coefficient of 0.998.

C. Lift-Induced Drag

The phase-averaged lift-induced drag was computed from the vorticity using the Maskell induced-drag model.[22,23] The phase-averaged vw-crossflow velocity vectors within the measurement plane were decomposed into a stream function $\psi(y, z)$ and a velocity potential $\phi(y, z)$ with the imposed boundary conditions requiring both ψ and ϕ to be zero on the edges of the measurement plane. The induced drag was then obtained by

$$D_i = \frac{1}{2}\rho_\infty \iint_{S_\zeta} \psi\zeta \, \mathrm{d}y \, \mathrm{d}z - \frac{1}{2}\rho_\infty \iint_{S1} \phi\sigma \, \mathrm{d}y \, \mathrm{d}z \qquad (3)$$

where ζ is the vorticity, the surface S_ζ is the region within $S1$ where the vorticity is nonzero, $\sigma (= \partial v/\partial y + \partial w/\partial z)$ is a source term, and the flow is incompressible. Figure 9 summarizes the values of the uncompensated and compensated lift-induced drag coefficient C_{Di} as a function of κ and x/c. The values of C_{Di} increased with α and κ (especially for $\kappa > 0.12$) but varied less noticeably with x/c in the near-wake region. The minima in the C_{Di} loops occurred when the circulation was zero, or at $\alpha(t)$ when the wing is generating zero lift. The maxima in the C_{Di} loops occurred when the tip vortex is strongest, which, notably, was not at the maximum α. The oscillating wing was found to generate higher induced drag than its static counterparts; depending on the reduced frequency, a 35 to 85% increase in the induced drag was generated for $\kappa = 0.09$ to 0.18. Furthermore, the values of C_{Di} were generally higher during pitch-down than during pitch-up for positive angles of attack; a result consistent with the observed trend in the vortex strength (Fig. 5).

IV. Conclusions

The effect of the reduced frequency on the phase-locked ensemble-averaged tip vortex structure behind a NACA 0015 airfoil oscillated within the static-stall angle (=14 deg) was investigated. The nearly symmetric vortex was observed for $x/c \geq 0.5$ for an oscillating wing, similar to the case of a stationary wing. Many of the vortex flow features, during both pitch-up and pitch-down, are qualitatively similar to those observed in the tip vortex behind a stationary wing. The peak values of the vortex flow quantities and the vortex strength and the lift-induced drag had higher values during pitch-down than during pitch-up. The level of hysteresis generally increased with the reduced frequency. The axial-flow velocity was wake-like with the minimum values increasing with the reduced frequency. The oscillating wing produced a less concentrated vortex of similar diameter and had a larger radial gradient in circulation strength, compared to a stationary wing. The normalized circulation within the inner region of the nearly symmetric tip vortex exhibited a self-similar structure, which was insensitive to the reduced frequency. The induced drag increased with the reduced frequency.

Acknowledgments

This work was supported by the Natural Sciences and Engineering Research Council of Canada.

References

[1]El-Ramly, Z., and Rainbird, W. J., "Flow Survey of the Vortex Wake Behind Wings," *Journal of Aircraft*, Vol. 14, No. 11, 1977, pp. 1102–1108.

[2]Shekarriz, A., Fu, T. C., Katz, J., and Huang, T. T., "Near-Field Behavior of a Tip Vortex," *AIAA Journal*, Vol. 31, No. 1, 1993, pp. 112–118.

[3]Devenport, W. J., Rife, M. C., Liapis, S. I., and Follin, G. J., "The Structure and Development of a Wing-Tip Vortex," *Journal of Fluid Mechanics*, Vol. 312, 1996, pp. 67–106.

[4]Chow, J. S., Zilliac, G. G., and Bradshaw, P., "Mean and Turbulence Measurements in the near Field of a Wingtip Vortex," *AIAA Journal*, Vol. 35, No. 10, 1997, pp. 1561–1567.

[5]Ramaprian, B. R., and Zheng, Y., "Measurements in Rollup Region of the Tip Vortex from a Rectangular Wing," *AIAA Journal*, Vol. 35, No. 12, 1997, pp. 1837–1843.

[6]Birch, D., and Lee, T., "Rollup and near-Field Behavior of a Tip Vortex," *Journal of Aircraft*, Vol. 40, No. 3, 2003, pp. 603–607.

[7]Birch, D., and Lee, T., "Structure and Induced Drag of a Tip Vortex," *Journal of Aircraft*, Vol. 41, No. 5, 2004, pp. 1138–1145.

[8]Birch, D., and Lee, T., "Effect of Trailing-Edge Flap on a Tip Vortex," *Journal of Aircraft* (to be published).

[9]Freymuth, P., Finaish, F., and Bank, W., "Visualization of Wing-Tip Vortices in Accelerating and Steady Flow," *Journal of Aircraft*, Vol. 23, No. 9, 1985, pp. 730–733.

[10]Ramaprian, B. R., and Zheng, Y., "Near Field of the Tip Vortex Behind an Oscillating Rectangular Wing," *AIAA Journal*, Vol. 36, No. 7, 1998, pp. 1263–1269.

[11]Chang, Y. W., and Park, S. O., "Measurement in the Tip Vortex Rollup Region of an Oscillating Wing," *AIAA Journal*, Vol. 38, No. 6, 2000, pp. 1092–1095.

[12]Lee, T., and Basu, S., "Measurement of Unsteady Boundary Layer Developed on an Oscillating Airfoil Using Multiple Hot-Film Sensors," *Experiments in Fluids*, Vol. 25, No. 2, 1998, pp. 108–117.

[13]Kowal, H. J., and Vakili, A. D., "Unsteady Vortex Breakdown Over a Pitching-Rolling 70° Delta Wing," *Canadian Aeronautics and Space Journal*, Vol. 46, No. 1, 2000, pp. 40–46.

[14]Lee, T., and Gerontakos, P., "Investigation of Flow over an Oscillating Airfoil," *Journal of Fluid Mechanics*, Vol. 512, 2004, pp. 313–341.

[15]McCroskey, W. J., Carr, L. W., and McAlister, K. W., "Dynamic Stall Experiments on Oscillating Airfoils," *AIAA Journal*, Vol. 14, No. 1, 1976, pp. 57–63.

[16]McCroskey, W. J., "Unsteady Airfoils," *Annual Review of Fluid Mechanics*, Vol. 14, 1982, pp. 285–311.

[17]Johnson, W., and Ham, N. D., "On the Mechanism of Dynamic Stall," *Journal of American Helicopter Society*, Vol. 17, No. 4, 1972, pp. 36–45.

[18]Wenger, C. W., and Devenport, W. J., "Seven-Hole Pressure Probe Calibration Utilizing Look-up Error Tables," *AIAA Journal*, Vol. 37, No. 6, 1999, pp. 675–679.

[19]Batchelor, G. K., "Axial Flow in Trailing Line Vortices," *Journal of Fluid Mechanics*, Vol. 20, 1964, pp. 645–658.

[20]Hoffmann, E. R., and Joubert, P. N., "Turbulent Line Vortices," *Journal of Fluid Mechanics*, Vol. 16, 1963, pp. 395–411.

[21]Phillips, W. R. C., "The Turbulent Trailing Vortex During Roll-Up," *Journal of Fluid Mechanics*, Vol. 105, 1981, pp. 451–467.

[22]Brune, G. W., "Quantitative Low-Speed Wake Surveys," *Journal of Aircraft*, Vol. 31, No. 2, 1994, pp. 249–255.

[23]Maskell, E., "Progress Towards a Method for the Measurement of the Components of the Drag of a Wing of Finite Span," Royal Aircraft Establishment, TR 72232, London, 1973.